Preprint- SPIE Smart Structures and Materials 2003- Paper # 5053-29

Effect of composition on the magnetic and elastic properties of shape-memory Ni-Mn-Ga

Aayush Malla [a], Marcelo Dapino[a], Thomas Lograsso[b], Deborah Schlagel[b]
[a]Department of Mechanical Engineering, Ohio State University, Columbus, OH 43210
[b]Department of Materials Science and Engineering, Iowa State University, Ames, IA 50011

ABSTRACT

The growing interest in ferromagnetic shape-memory Ni-Mn-Ga for implementation in actuator applications originates from the fact that this class of materials exhibits large strains when driven by a magnetic field. Large bidirectional strains up to a theoretical 6% are produced in these materials by twin boundary motion as martensite variants rotate to align respectively parallel or perpendicular to applied magnetic fields or stresses. These strains represent a significant improvement over piezoelectric and magnetostrictive materials. In this paper, we report on experimental measurements conducted on Ni-Mn-Ga cylindrical rods subjected to uniaxial stresses and uniaxial magnetic fields which were applied *collinearly* along the magnetic easy axis direction of the rods. To this end, a test apparatus was developed which consists of a water-cooled solenoid actuator and a loading fixture. Despite the lack of a readily recognizable mechanism for reversible deformations, bidirectional strains as large as 4300 ppm (0.43%) were observed, or three times the saturation magnetostriction of Terfenol-D. This paper presents room-temperature data including magnetization hysteresis, strain versus field and peak strain versus stress curves collected over a range of stresses between 0-65 MPa. From the latter set of curves, blocking force values are estimated as those for which the strain is 1% of the maximum (zero-load) strain. The results illustrate the sensitivity of material behavior with respect to composition at different driving conditions and offer insight on the choice of material compositions at which maximum actuation performance is achieved.

Keywords: Ferromagnetic shape memory, twin boundary motion, cubic to tetragonal transformation, magnetic field-induced strain, coercive field, remanent magnetization.

1. INTRODUCTION

In Ni_2MnGa ferromagnetic shape memory alloys, cooling below the characteristic martensite start temperature M_s produces a cubic to tetragonal transformation and a corresponding twin-variant structure. Either magnetic fields or stresses can be used to bias these materials toward one martensite variant or the other, which results in twin boundary motion and ensuing deformations as variants rotate to align respectively parallel or perpendicular to the field or stress direction. Bidirectional deformations are obtained through field or stress rotation, or more typically, by driving these materials with an alternating uniaxial magnetic field oriented orthogonal to a fixed uniaxial stress. The significance of Ni_2MnGa lies in its broader bandwidth compared to conventional thermally activated shape memory materials.

Over a certain compositional range, the martensite structure is tetragonal with c/a=0.94, thus the theoretical relative strain obtained from this structure is approximately 6%. The high temperature austenite Heusler phase exists over wide compositional ranges, centered on Ni_2MnGa, over which the magnetic properties and martensite transformation temperature vary continuously. Furthermore, depending on the composition, several different martensite structures have been reported. These variations in properties have been compiled onto the compositional map shown in Fig. 1, [5] which plots saturation magnetization, Curie temperature and martensite start temperatures. It has been speculated, based on a minimum saturation magnetization of 60 emu/g and martensite transformation temperatures above 300K, that compositions within the shaded region would exhibit the largest magnetic-field induced strains. Experimentally, alloys lying just to the right and above the shaded region have been found to exhibit the largest magnetic field-induced strains [10]. In this paper, we examine the response of alloys whose compositions are lower in

(AM) malla.1@osu.edu; Ph.: (614) 247-7480
(MD) (Correspondence) dapino.1@osu.edu; Ph.: (614) 688-3689
(TL) lograsso@ameslab.gov; Ph.: (515) 294-8425
(DS) schlagel@iastate.edu; Ph.: (515) 294-3924

Ga and higher in Mn than those believed to exhibit largest field-induced strains (squares in Fig. 1). More importantly, in the experiments presented here, a uniaxial stress and uniaxial magnetic field were applied *collinearly* along the magnetic easy axis direction of the samples, contrary to the conventional perpendicular arrangement. Despite the lack of a known mechanism for bidirectional twin boundary motion, reversible strains as large as 4300 ppm (0.43%) were obtained. These reversible field-induced strains are too large to result from Joule magnetostriction (typically only 250 ppm for these alloys) nor can they be explained by the existing martensite variant reorientation models. Furthermore, contrarily to the conventional processing practice of material training through field cycling and thermal treatments, these large strains were observed in samples tested as cast. The significance of the experimental data presented in this paper is that a collinear drive configuration facilitates the use of solenoids for field actuation, as opposed to electromagnets as is conventionally the case (Fig. 2(a)). Solenoids present several advantages over electromagnets including significantly reduced size and weight as well as broader frequency bandwidth.

Despite the small changes in composition between the alloys investigated in this paper and those showing the largest magnetic field-induced strains, significant and profound differences are apparent between the two. It has been recently reported that the room temperature structure of the martensite phase at higher Mn content is orthorhombic (c/a=1.1) rather than tetragonal [15]. A second and perhaps more significant property of the samples investigated here is that the shape memory martensite transformation temperatures are nearly coincident with the ferromagnetic ordering temperature, suggesting a coupled magneto-structural transformation which may be responsible for the observed reversible strains. Coupled transitions, known to exist in rare-earth-silicon-germanium compounds [13,14], result in extraordinary magnetic responses including large magnetostriction, where application of a magnetic field drives the structural change from a paramagnetic austenite phase to a ferromagnetic martensite phase. This structural change is fully reversible when the magnetic field is removed.

In order to gain a fundamental understanding and ultimately develop constitutive models of the magnetoelastic and thermoelastic behavior exhibited by these alloys, the dependence of the magnetic and physical properties on the composition and structural characteristics of the shape memory transformation must be elucidated. This paper presents the first step toward that end by presenting room-temperature magnetization and strain measurements for Ni-Mn-Ga alloys centered on $Ni_{49.5}Mn_{29.5}Ga_{21}$ under quasistatic fields of amplitude 8.1 kOe (650 kA/m). The ability of these alloys to produce mechanical work is evaluated through strain measurements at constant stress for a range of compressive stresses between 0-65 MPa. Dynamic experimental results presented in [1] involving broadband frequency response behavior in the dc-20 kHz range and elastic moduli calculations from resonant response under various bias fields, suggest the presence of a Delta-E effect similar to that observed in Terfenol-D when Ni-Mn-Ga alloys are driven by a collinear magnetic field-stress pair. Furthermore, stiffness calculations shown in [1] suggest that solenoid-driven Ni-Mn-Ga alloys could exhibit significantly higher stiffnesses than those previously measured employing conventional electromagnet tests (30 GPa versus 7 GPa.).

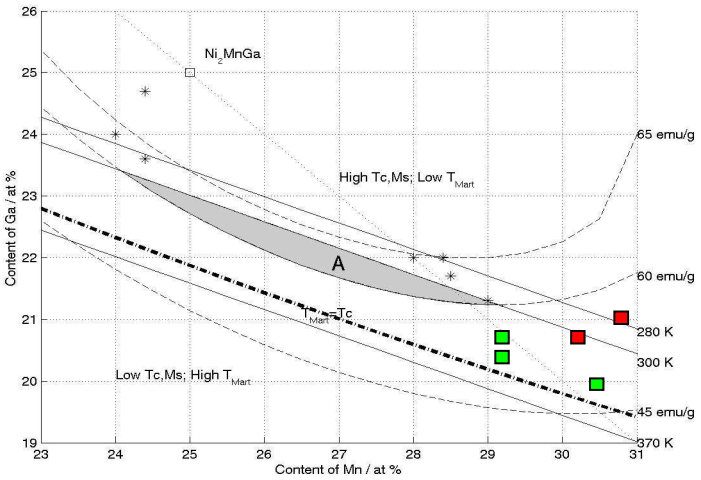

Figure 1: Compositional map for Ni-Mn-Ga ferromagnetic shape memory alloys, taken from Jin et al. [5]. The square symbols show the compositions examined in this paper.

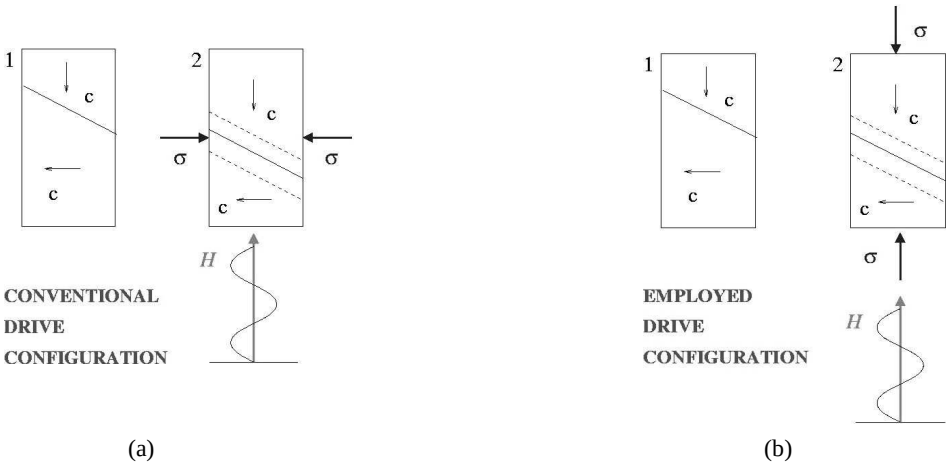

(a) (b)

Figure 2: (a) Electromagnet-based drive configuration. (b) Solenoid-based drive configuration employed here.

2. MATERIAL PREPARATION AND PROPERTIES

Five cylindrical samples of various parent phase compositions where tested. Each sample was prepared as follows. Appropriate quantities of high purity nickel, manganese and gallium were cleaned and arc melted several times under an argon atmosphere. The buttons were remelted and the alloy drop cast into a chilled copper mold to ensure compositional homogeneity throughout the ingot. The crystal was grown from the as-cast ingot in an alumina Bridgman style crucible which was heated to 1350ºC under a pressure of 1.3×10^{-4} Pa to degas the crucible and charge. After melting, the chamber was backfilled to a pressure of 2.76×10^{5} Pa with high purity argon to eliminate gas pockets and to minimize the amount of manganese evaporation from the melt during the crystal growth. The ingot was held at 1350ºC for 1 hour to allow thorough mixing before withdrawing the sample from the heat zone at a rate of 5 mm/hr. Cylindrical samples measuring 0.25" (6.35 mm) in diameter were extracted from the crystal boule by electric discharge milling, and their composition measured along the longitudinal axis by energy dispersive microanalysis. Because the composition is known to vary along the boule axis with Mn content increasing and Ga content decreasing in the growth direction, the tested samples were taken from the top and bottom of each boule for maximum compositional variation within each boule. Table 1 shows the characteristic temperatures for the tested samples while Table 2 shows the compositions in percentage by atomic weight for the different samples.

Table 1: Characteristic temperatures in ºC for the tested samples.

Sample ID	Rod#	As(1[a])	Af(1)	Ms(1)	Mf(1)	As(2[b])	Af(2)	Ms(2)	Mf(2)	Tc heating	Tc cooling
dls-1-125	4,top	33.1	87.7*	77.7	-					87.7	87.0
	4,bottom	37.5	54.4	45.4	20.0					96.9	94.6
dls-1-61	1,top	49.5	64.1	54.2	43.0					96.7	94.5
	1,bottom	43.0	69.8	61.0	40.7					97.0	95.4
dls-1-42	1,top	49.8	111.1*	106.7**	60.8					111.1	106.7
	1,bottom	+	100.2	90.0**	60.4	52.7	+	4.7	-23.9	100.2	90.0
	2,top	+	113.6*	108.4	76.9	47.4	+	-11.6	-49.5	120.2	114.9
	2,bottom	76.6++	103.6	94.4	65.6	49.2	67.0++	-4.6	-23.2	103.6	99.4
	3,top	80.7++	118.5	108.8	77.2	53.7	71.4++	-21.2	-51.2	124.6	119.5
	3,bottom	+	104.4	95.6	73.6	48.4	+	-4.5	-26.4	112.2	107.6

[a] High temperature martensite transformation, [b] Low temperature martensite transformation, * Af =Tc, ** Ms=Tc
+ Af(2) and As(1) overlap, ++ Af(2) and As(1) overlap on one cycle only.

Table 2: Compositions in percentage by atomic weight of nickel, manganese and gallium for the five samples tested in the study.

Sample	Mn	Ni	Ga	e/a*	Length (inches)
dls-1-125-4	30.60	48.10	21.30	7.951	1.025
dls-1-61-1	29.98	48.99	21.03	7.629	0.954
dls-1-42-1	30.40	49.54	20.06	7.684	0.840
dls-1-42-2	28.91	50.52	20.57	7.693	0.842
dls-1-42-3	28.97	50.20	20.84	7.673	0.851

*e/a = (7Mn+10Ni+3Ga)

3. EXPERIMENTAL SETUP

3.1 Test Apparatus

The experimental data were obtained from the test apparatus shown in Fig. 3, which consists of a broadband solenoid-based transducer and a fixture that provides static uniaxial stresses by means of dead weights. The transducer houses one cylindrical sample of dimensions up to 0.5”-diameter by 4.5”-length and is configured for d_{33} actuation mode with the longitudinal axis of the sample, magnetic field, and uniaxial stress aligned collinearly.

The transducer consists of several parts made from magnetic and non magnetic materials for efficient flux flow. As illustrated in Figs. 3(b) and 4, the housing comprises a cylindrical housing and top and bottom plates made from 1018 steel. A 1018 magnetic steel base is screwed to the bottom plate and a bottom cap made from stress proof 1144 steel is fixed to the magnetic steel base. A 6061 T6 hollow aluminum spool and sensing solenoid sit inside a sample holder made of 304 stainless steel. The sample holder has internal threads at the bottom and is screwed to the external threads of the bottom cap. A linear motion bearing is press fit on the top of the sample holder to support the motion of the pushrod with minimum friction and for closing the magnetic circuit formed by the Ni-Mn-Ga sample, top and bottom plates and caps, and transducer housing.

The drive fields are provided by a water-cooled solenoid consisting of AWG15 insulated copper wire wound in 28 layers with approximately 48 turns per layer. A cooling/heating circuit of 0.25in-diameter copper tube is interspersed within the solenoid and high performance epoxy Epotek T7109 provides structural support to the assembly. Water is circulated in the system at a rate and temperature regulated by means of a water mixer. The temperature at different locations in the transducer is monitored by Omega thermocouples connected to a 10-channel Omega signal conditioner. For all of the tests, the sample temperature was maintained at 14°C. The solenoid is driven by two Techron 7790 amplifiers connected in series which produce an overall voltage gain of 60 and maximum output current of 56 A at the rated coil resistance of 3.7 Ohms (11.6 kW). The magnetic induction is measured with a pickup coil made from AWG33 grade insulated copper wire wound several layers around the aluminum spool and connected to a Walker Scientific MF-5D integrating fluxmeter which directly converts the change in voltage across the sensing coil to magnetic induction.

Since the Ni-Mn-Ga samples are more than an inch shorter than the height of the solenoid, two magnetic stress proof 1144 steel pieces of equal length were attached with wax at to the top and bottom of the samples thus aiding in positioning the sample symmetrically at the center of the solenoid's longitudinal axis. Compressive loading is applied to the samples through a pushrod made of 1144 stress-proof magnetic steel connected to a steel cross bar with an interface piece of non-magnetic 304 stainless steel in between to prevent the magnetic flux lines from leaking out. A second cross bar connected to the top cross bar by means of vertical non-magnetic steel rods provides a means for hanging a set of interconnecting steel trays which hold lead bricks. The vertical rods slide in low-friction linear motion bearings which are rigidly attached to the fixture frame. The number of trays and lead bricks connected to the transducer’s load path can be varied such that the compressive force on the sample is adjusted from zero up to a maximum of 1.5 kip (6.6 kN) in virtually continuous increments. A PCB 208C04 force transducer is located between the cross bar and the interface piece of non-magnetic steel, and is used to monitor the compressive force applied to the Ni-Mn-Ga sample. The strain is measured by a Lucas Shaevitz MHR-025 linear variable differential transducer. Fig. 4 shows the cross section of the transducer without the loading fixture. The input and output signals are generated by and recorded through a Data Physics SignalStar Vector 550 dynamic signal analyzer that is interfaced through a PC.

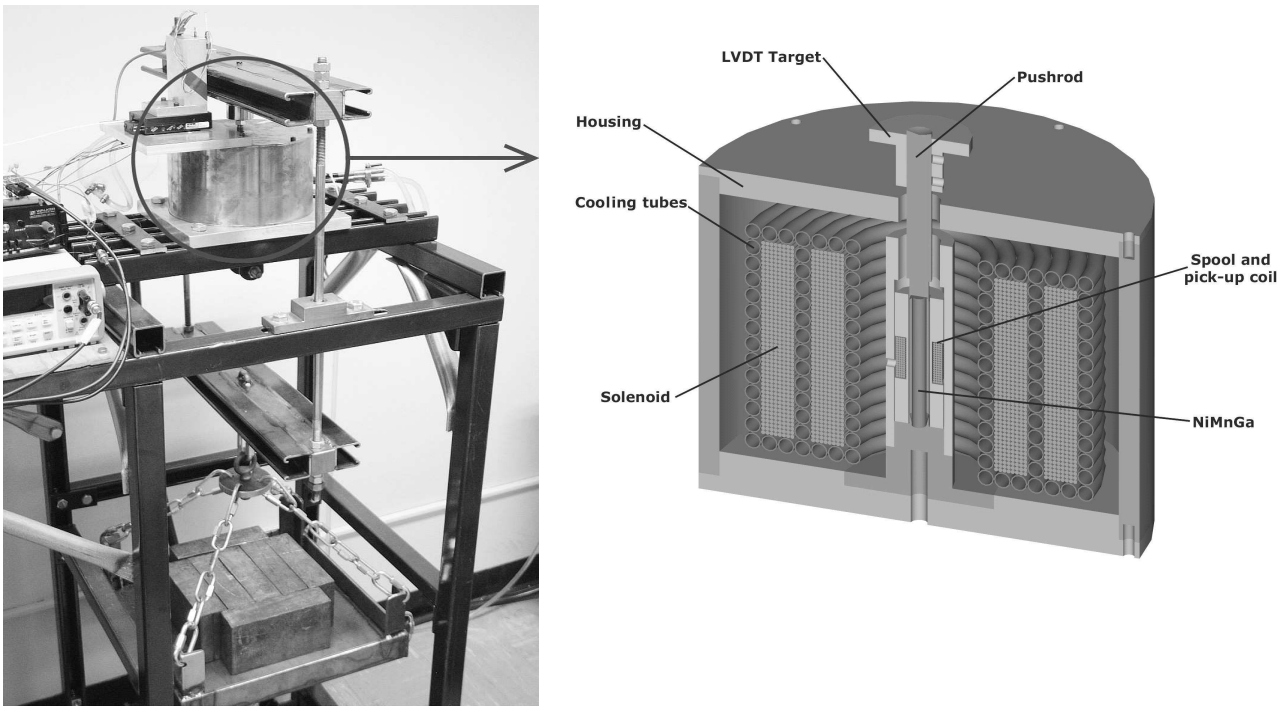

(a) (b)

Figure 3: (a) Fixture employed for testing Ni-Mn-Ga samples with a collinear magnetic field-stress pair. (b) Three dimensional sectioned view of the main transducer showing the interior.

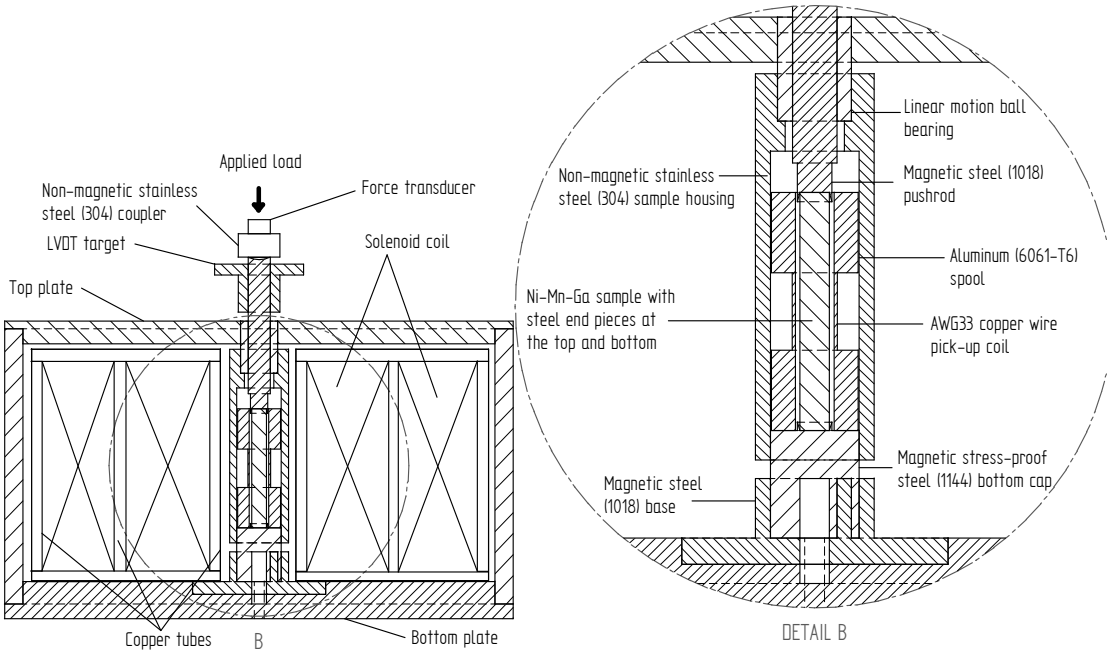

Figure 4: Cross sectional view of the water-cooled transducer used for testing of the Ni-Mn-Ga samples.

3.2 Solenoid Calibration

The magnetic field intensity produced by the transducer at maximum drive current was determined employing three different techniques and the effective field per current was then estimated from the average of the three techniques. The techniques include low frequency experimental measurements, magnetostatic finite element analysis and thick-solenoid equations. Magnetodynamic effects are neglected consistently with the fact that the material characterization tests were conducted at low frequency (0.1 Hz) sinusoidal excitations. For the experimental tests, a Walker Scientific MG-4D Gaussmeter with an HP 245S axial Hall probe was used for measuring the magnetic field intensity along the axis of the main solenoid at different dc current intensities. This method gives a mean field per current constant equal to 150 Oe/A. The actual value is estimated to be larger than this since the above procedure requires the removal of the transducer pushrod thus implying a greater amount of leakage flux than normal.

The magnetostatic finite element characterization was conducted on the freeware package FEMM 3.2 in which a 2-D axisymmetric geometry was assumed. The current density employed in the FEM simulations was determined by considering the magnetic flux density at strategic locations in the transducer when the active sample is replaced with known materials such as AISI 1018 steel or air. A sample output from the software is illustrated in Fig. 5. The variation of magnetic field intensity along the longitudinal axis of the sample as computed by the software for the maximum drive amplitude is shown in Figure 6. The total effective number of wire turns was estimated at 1325 taking into account the losses due to uneven packing at the top and bottom of the solenoid and due to the space occupied by the epoxy between the windings. The total cross sectional area occupied by the solenoid was measured from the dimensions and found to be 44.6×10^{-4} m^2. The current density was calculated in this manner rather than dividing the current flowing in the wire by the cross sectional area of a single wire because of the considerable number of uneven windings. The FEMM 3.2 calculations give an average value of 175 Oe/A for the field per current rating of the transducer.

Finally, thick-solenoid equations were also considered as a means for complementing the experimental and computational results described above. For a thick solenoid of N turns, length L, inner radius r_1 and outer radius r_2 excited by a current I, the field intensity at the center of the solenoid has the form [9]

$$H_0 = F(\alpha, \beta)\, f(I, r_1, r_2), \tag{1}$$

where the functions $F(\alpha, \beta)$ and $f(I, r_1, r_2)$ which respectively represent a field factor and a current factor are given by

$$F(\alpha, \beta) = \beta\, [\text{arsinh}\, (\alpha/\beta) - \text{arsinh}\, (1/\beta), \tag{2}$$

$$f(I, r_1, r_2) = (N\, I / L)\ \ [r_1/(r_2 - r_1)]. \tag{3}$$

Here, $\alpha = r_2 / r_1$, $\beta = L/(2\, r_1)$ represent normalized geometric coefficients.

For a solenoid with N = 1325 turns, inner radius r_1 =1.06", outer radius r_2 =3.3" and length L =3.4", relations (1)-(3) yield a field per current rating of 160 Oe/A. Based on the three calibration techniques described here in combination with additional experimental testing performed on known materials such as nickel, 1018 steel and Terfenol-D, it has been determined that the effective rating of the solenoid is 167 Oe/Amp. This value was subsequently used for the determination of the applied magnetic fields from measured current signals, i.e., $H(t) = 167\, I$ Oe.

4. EXPERIMENTAL DATA AND ANALYSIS OF RESULTS

The fundamental objective of this investigation is to determine whether or not it is possible to magnetically induce twin boundary motion in cylindrical Ni-Mn-Ga samples subjected to a collinear magnetic field-stress pair. To this end, five rods of composition as described in Table 2 were subjected to unbiased sinusoidal magnetic fields with frequency of 0.1 Hz and 0-pk amplitude of 8.1 kOe (650 kA/m). Displacement, force and magnetic induction measurements were collected at constant mechanical load for various loads ranging from nearly zero to 65 MPa. The lowest loading condition is defined by the pushrod weight, i.e., 39 g.

In this paper, we present strain versus magnetic field, magnetization versus field and peak strain versus stress curves. The strain for each sample was determined by $e(t) = \Delta L / L$ and the stress by $\sigma(t) = F / A$, where ΔL and F denote respectively the LVDT signal and force transducer signal, and L and A are the length and cross sectional area of each rod. The magnetization was determined from the magnetic induction and field by $M(t) = B / \mu o - H$, where $H(t)$ is the

field determined from the measured current as discussed in Section 3.2, *B(t)* is the measured magnetic flux density and $\mu o = 4\pi \times 10^{-7}$ H/m is the permeability of free space. It is noted that a blocking force value has been defined as the mechanical load at which the peak strain of any given sample is 1% of the peak strain at zero load, i.e., the largest strain possible for that sample. It is immediately apparent from the curves shown in Figs. 7-9 and summarized in Table 3 that $Ni_{48.1}Mn_{30.6}Ga_{31.3}$ (sample dls-1-125-4) and $Ni_{49}Mn_{30}Ga_{21}$ (sample dls-1-61-1) are the most interesting compositions as they exhibit substantially larger strains than the other samples. Moreover, the data for the least active samples (dls-1-42-1, 2, 3) show peak strains which are comparable to the Joule magnetostriction for these alloys, suggesting that for these three samples the observed strains are not caused by twin boundary motion.

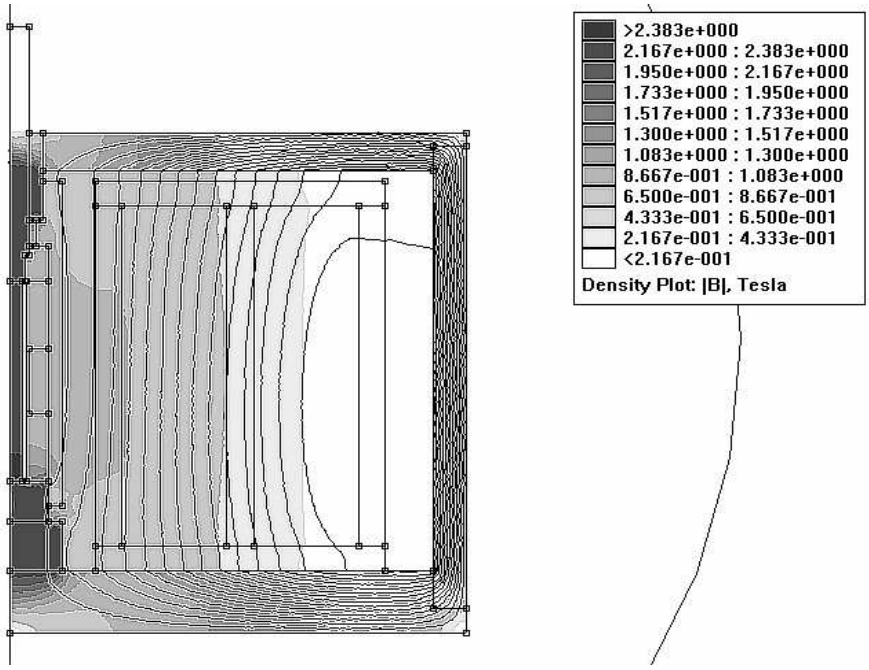

Figure 5: Axisymmetric FEM output showing the magnetic flux density distribution and flux line contours in the transducer in which 1018 steel is used as the test sample.

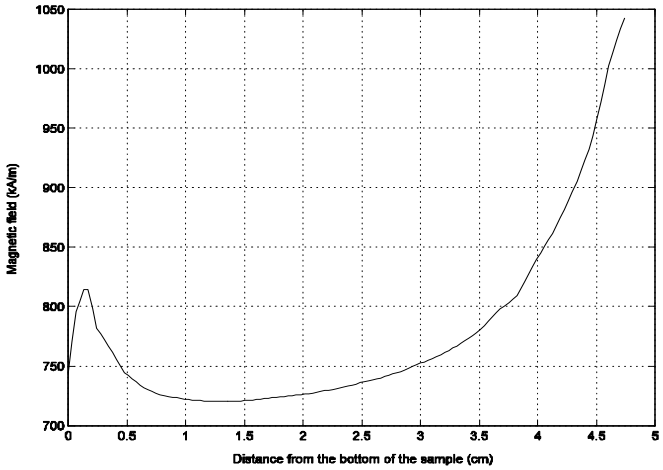

Figure 6: Axisymmetric FEM calculation of the magnetic field intensity along the centerline of an AISI 1018 steel rod, where x=0 represents the bottom of the rod.

Figure 7 shows a series of measurements at 0.1 Hz drive frequency for the most active sample, dls-1-125-4. The zero-load strain versus field curve is shown in Fig. 7(a). It is emphasized that a very large peak deformation of 4300 ppm (0.43%) has been obtained, or three times the saturation magnetostriction of Terfenol-D. The crossover point for this curve is 621.4 ppm. The crossover point is here defined as the strain at which the value of the magnetic field is zero or equivalently, the point of contact of the two halves of the "butterfly" curve. A significant amount of hysteresis is observed. The corresponding no-load magnetization curve, plotted in Figure 7(b), shows a saturation magnetization close to 342.8 kA/m. The remanent magnetization and coercive field values are 171.25 kA/m and 8.25 kA/m, respectively. The effect of compressive load on the strain is shown in Figs. 7(c)-(d) in which the peak field is fixed. Including the zero load case, a total of 19 fixed-stress curves are shown. As expected, both the peak value and the crossover point decrease in magnitude with increasing load. In Figs. 7(e), we illustrate the effect of stress on strain by plotting the peak strain obtained in each of the 19 loading cases as a function of the stress load. Because each strain curve was collected at constant stress, this graph is representative of the dependency of mechanical work produced by the Ni-Mn-Ga sample with external load. This dependency is shown to be exponential. Notwithstanding, the peak strain at a stress of 6.9 MPa (1 ksi) has a value near 1000 ppm, that is comparable to the mechanical work output of terfenol. Figure 7(f) shows a detail of the induction versus field curve for all of the load values. It is seen that the induction is different in the unloaded case with lower remanence and coercivity as compared to the induction for the loaded cases where the two parameters seem to remain almost constant. This trend seemingly contradicts the law of approach to the anhysteretic magnetization observed in ferromagnetic materials under increasing compressive or tensile stress [4].

Figure 8 shows a corresponding set of graphs for dls-1-61-1 as tested at 0.1 Hz drive frequency. The sample produced a peak field-induced strain of 1192 ppm at no load with a crossover point of 198 ppm, as shown in Fig. 8(a). It is noted that although this peak strain is about four times smaller than that for dls-1-125-4, the magnetization figures of merit for both samples do not differ nearly as much. As shown in Fig. 8(b), the saturation magnetization has a value of 371.6 kA/m while the remanent magnetization and coercive field values are respectively 222.97 kA/m and 8.87 kA/m. These results highlight that the observed strains are not directly linked to the magnetization as is the case with Joule magnetostriction, hence suggesting that the deformations are due to a different and more powerful phenomenon, such as twin boundary motion. Figs. 8(c)-(d) show the strain versus field curves for mechanical loads up to 465 lbs (65.5 MPa). The strain decreases with increasing load in an exponential manner as illustrated in Fig. 8(e). Figure 8(f) shows a detail of the magnetic induction versus field curve for loads up to 366 lbs (51.5 MPa) at steps of 24 lbs starting from 0 lbs. The remanent induction and coercive field are almost constant and no significant change is observed between the magnetic induction curves in the various loading cases.

The dls-1-42 series samples were also driven with a 0.1 Hz unbiased sinusoidal magnetic field of 0-pk amplitude equal to 8.1 kOe (650 kA/m). The strain data indicate very weak actuation of 240, 215 and 177 ppm, respectively for samples dls-1-42-1, 2 and 3, which are very low compared to the strains exhibited by the other samples. Furthermore, the percentage error in the strain measurements for these samples is expected to be higher because of the weak strain produced and the steel end pieces themselves being magnetostrictive. The steel end pieces along with other steel components in the transducer were observed to produce 40-50 ppm with the reversal of strain direction at about 300 kA/m, thus exhibiting a typical "W" shape. Subtraction of the steel magnetostriction from the strain measurements from the dls-1-42 series samples producing low strain would result in a significant magnitude of error. These three samples were also tested at higher loads under the same conditions as dls-1-125-4 and dls1-61-1 but due to the aforementioned reason, the data has not been included in the paper. Figure 9(a) shows the magnetization curve for dls-1-42-1. The saturation magnetization is about 349.8 kA/m and the remanent magnetization and coercive field are 214.85 kA/m and 8.17 kA/m, respectively. Figure 9(b) shows the change in coercivity and remanent induction with increase in load for dls-142-3, which was the most significant among all the samples investigated. It can be inferred from the plots that the remanent magnetization first decreases with loading of 50 lbs (7.03 MPa) after which it increases gradually at higher loads. At higher loads, the increase in remanence is not as significant as for lower loads. However, the change in coercive field is very small and not discernible and a trend may not be possible to define.

Finally, Fig. 10 shows experimental and calculated saturation magnetization values for Ni-Mn-Ga alloys as a function of e/a ratio, taken from the literature [5], as well as the measurements obtained in our experiments. It is noted that the value of saturation magnetization for the most active of our samples, dls-1-125-4, is very close to the value defined by the linear fit show in Fig. 10. Moreover, our experimental magnetic saturation value of dls-1-125-4 is very close to the experimental value of a sample with almost the same e/a ratio, marked + in Fig. 10. Such a close match is remarkable and not seen in the other samples. A summary of the measurements presented here is provided in Table 3.

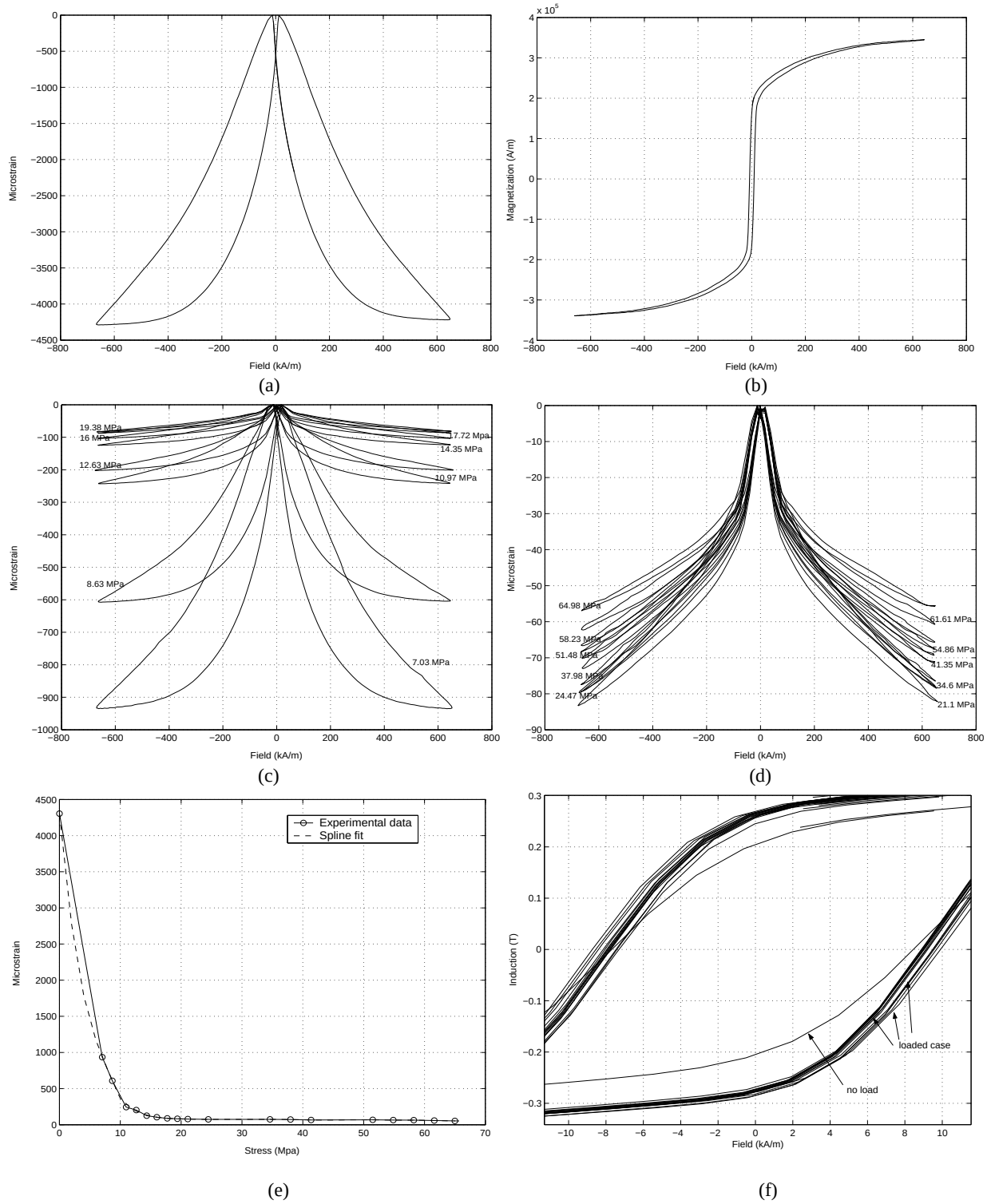

Figure 7: Measurements for $Ni_{48.1}Mn_{30.6}Ga_{31.3}$ (sample dls-1-125-4). (a) Zero-load strain vs. field. (b) Corresponding magnetization vs. field curve. (c), (d) Strain vs. field for a range of compressive stresses from 7-65 MPa. (e) Peak strain vs. stress taken from (c) and (d). (f) Detail of magnetic induction vs. field for loads from 0-390 lbs at 24 lb steps.

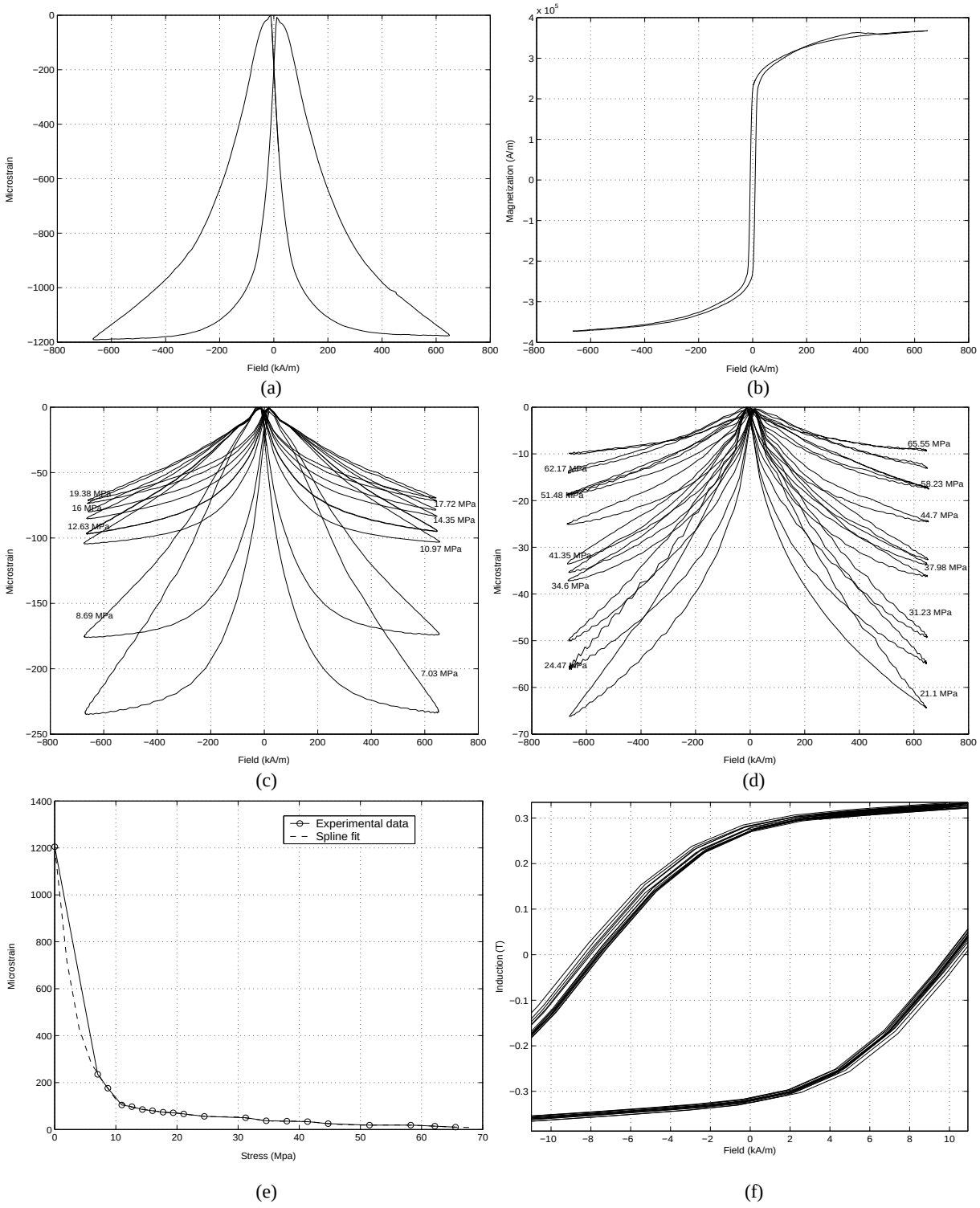

Figure 8: Measurements for $Ni_{49}Mn_{30}Ga_{21}$ (sample dls-1-61-1). (a) Zero-load strain vs. field. (b) Corresponding magnetization vs. field curve. (c), (d) Strain vs. field for a range of compressive stresses from 7-65 MPa. (e) Peak strain vs. stress taken from (c) and (d). (f) Detail of magnetic induction vs. field for loads from 0-65 MPa.

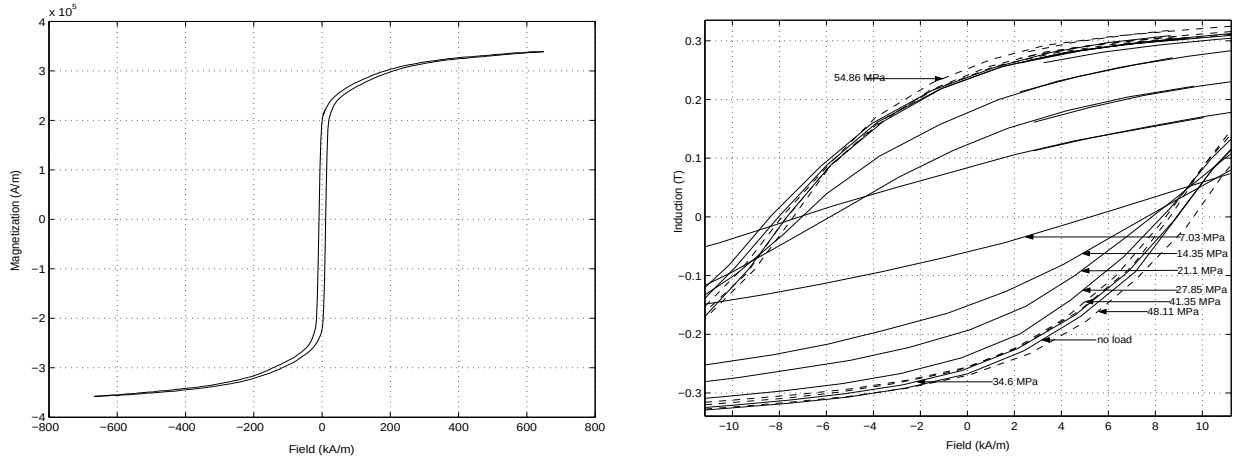

(a) (b)

Figure 9: (a) Zero-load magnetization curve for dls-1-42-1 under no load. (b) Detail of magnetic induction vs. field curves for dls-142-3 for loads 0-390 lbs at steps of 24 lbs.

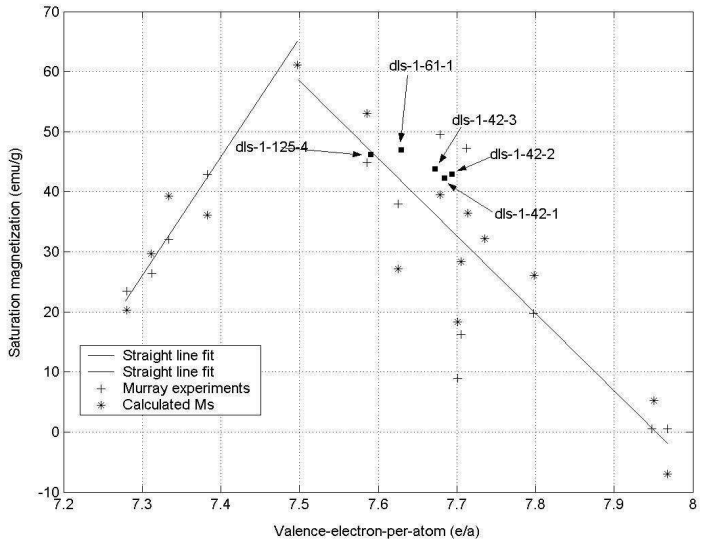

Figure 10: Experimental and calculated saturation magnetization mapping for Ni-Mn-Ga alloys as a function of e/a ratio (taken from [5]) as well as the measurements obtained in our experiments.

Table 3: Summary of experimental measurements presented in the paper.

Property	dls-1-125-4	dls-1-61-1	dls-1-42-1	dls-1-42-2	dls-1-42-3
Coercive field (kA/m)	8.25	8.87	8.17	7.6	7.56
Remanent magnetization (kA/m)	171.25	222.97	214.85	206.9	206.90
Relative permeability	28.26	40	37.89	39.15	37.98
Mean d_{33} increasing field (A/m)	1.08E-08	5.19E-09	-	-	-
Mean d_{33} decreasing field (A/m)	3.99E-08	2.00E-08	-	-	-
Crossover point (ppm)	621.40	198	-	-	-
Zero-load peak strain (ppm)	4300	1192	240	215	177

5. CONCLUDING REMARKS

In this paper, we have reported on experimental measurements conducted on Ni-Mn-Ga cylindrical rods subjected to a uniaxial stress-uniaxial magnetic field pair applied collinearly along the magnetic easy axis of the rods. A test apparatus was developed which consists of a water-cooled transducer and a loading fixture. The tested alloys have compositions that are lower in Ga and higher in Mn than those believed to exhibit largest field-induced strains. Strain measurements suggest the presence of very large magnetically-activated deformations of up to 4300 ppm (0.43%) for one of the compositions, i.e., $Ni_{48.1}Mn_{30.6}Ga_{31.3}$ (sample dls-1-125-4). The second-most active alloy, $Ni_{49}Mn_{30}Ga_{21}$ (sample dls-1-61-1), exhibits a peak strain of 1192 ppm. These deformations are seemingly too large to result from Joule magnetostriction, typically only 250 ppm for these alloys, nor can they be explained by the existing martensite reorientation models. Furthermore, the observed strains do not seem to be directly linked to the magnetization since all five samples exhibited comparable magnetization response despite the significant difference in strain among them. Another remarkable result is that for the most active alloy, the remanent induction and coercive field increase with increasing stress, seemingly contradicting the "law of approach" to the anhysteretic magnetization for ferromagnetic materials. The above observations suggest that despite the lack of a readily recognizable mechanism for twin boundary motion in Ni-Mn-Ga alloys tested in a collinear magnetic field-stress pair, a mechanism other than domain rotation may be responsible for the observed strains. In these alloys, twin boundary motion could stem from magneto-structural transformations evidenced by the fact that for these compositions the martensite transformation temperatures are nearly coincident with the ferromagnetic ordering temperatures. Coupled transitions, known to exist in rare-earth-silicon-germanium compounds, result in extraordinary magnetic responses including large magnetostriction and a structural change. This structural change is fully reversible when the magnetic field is reversed.

ACKOWLEDGEMENTS

Funding for AM and MD comes from the Ohio State University through startup funds. The authors wish to thank Prof. Richard James for helpful discussions.

REFERENCES

1. L. E. Faidley, M. J. Dapino, G. N. Washington, R. Smith, and T. A. Lograsso, "Analytical and experimental issues in Ni-Mn-Ga transducers," *Proc. SPIE Smart Structures and Materials*, Paper #5049-1, San Diego, CA, March 2003. To appear.
2. C.P. Henry, Jorge Feuchtwanger, David Bono, R.C. O'Handley, S.M. Allen, "AC magnetic field-induced strain of single crystal NI-Mn-Ga," *Proc. SPIE Smart Structures and Materials*, Vol. **4699**, pp.164-171, San Diego, CA, March 2002.
3. D. Jiles, *Introduction to Magnetism and Magnetic Materials*, Chapman and Hall, 1st edition, London 1998.
4. D. Jiles, "Theory of the magnetomechanical effect," *J. Phys. D (Appl. Phys.)*, 28:1537, 1995.
5. X. Jin, M. Marioni, D. Bono, S. M. Allen, and R. C. O'Handley, "Empirical mapping of Ni–Mn–Ga properties with composition and valence electron concentration," *J. Appl. Phys.*, Vol **91**(10), pp. 8222-8224, May 2002.
6. R. Kellogg and A. Flatau, "Blocked Force Investigation of a Terfenol-D transducer," *Proc. SPIE Smart Structures and Materials*, Vol. **3668**, pp. 184-195, Newport Beach, CA, March 1999.
7. A.A. Likhachev, A. Sozinov, and K. Ullakko, "Influence of external stress on the reversibility of magnetic-field-controlled shape memory effect in Ni-Mn-Ga," *Proc. SPIE Smart Structures and Materials*, Vol. **4333**, pp. 197-206, San Diego, CA, March 2002.
8. A.A. Likhachev, A. Sozinov, and K. Ullakko, "Optimizing work output in Ni-Mn-Ga and other ferromagnetic shape memory alloys," *Proc. SPIE Smart Structures and Materials*, Vol. **4699**, pp. 553-563, San Diego, CA, March 2002.
9. D. B. Montgomery, *Solenoid MagnetDesign*, Robert Krieger, New York 1980.
10. S.J. Murray, M. Marioni, S.M. Allen, R.C. O'Handley, and T.A. Lograsso, "6% magnetic-field-induced strain by twin boundary motion in ferromagnetic Ni-Mn-Ga," *Appl. Phys. Lett.*, Vol. **77**(6), pp. 886-888, August 2000.
11. S.J. Murray, M. Farinelli, C. Kantner, J.K. Huang, S.M. Allen, and R.C. O'Handley, "Field-induced strain under load in Ni-Mn-Ga magnetic shape memory materials," *J. Appl. Phys.*, Vol. **83**(11), pp. 7297-7299, June 1998.
12. R.C. O'Handley, S.J. Murray, M. Marioni, H. Nembach, and S.M. Allen, "Phenomenology of giant magnetic-field-induced strain in ferromagnetic shape-memory materials (invited)," *J. Appl. Phys.*, Vol. **87**(9), pp. 4712-4717, May 2000.
13. V. K. Pecharsky and K. A. Gschneidner, Jr., "Tunable magnetic regenerator alloys with a giant magnetocaloric effect for magnetic refrigeration from ~ 20 to ~ 290 K," *Appl. Phys. Lett.*, Vol. **70**(24), pp. 3299-3301, June 1997.
14. V. K. Pecharsky and K. A. Gschneidner, Jr., "Giant magnetocaloric effect in $Gd_5(Si_2Ge_2)$," *Phys. Rev. Lett,*,Vol. **78**(23), pp. 4494-4497, June 1997.
15. A. Sozinov, A. A. Likhachev, N. Lanska, and K. Ullakko, "Giant magnetic-field-induced strain in NiMnGa seven layered martensitic phase," *Appl. Phys. Lett.*, Vol. **80**(10), pp. 1746-1748, March 2002.